Dynamic Response of Magnetically Suspended Rotor under Base Motions

Yue ZHANG [a], Jin ZHOU [a], Jarir MAHFOUD [b], Yuanping XU [a], Yibo ZHANG [a]

a Nanjing University of Aeronautics and Astronautics, Yudao Street 29, 210016 Nanjing, China, zhangyue08@nuaa.edu.cn

b University of Lyon, INSA-Lyon, CNRS UMR5259, LaMCoS, F-69621 Villeurbanne Cedex, France

Abstract

Active magnetic bearings (AMBs) can provide no-friction support and active vibration control for rotating machinery. The magnetically suspended rotor will inevitably be excited by the base motions when working on the moving carrier, causing the rotor vibration, and even instability. The main purpose of this study is to investigate the vibration response of the magnetically suspended rotor under base motions, especially base rotation, and to evaluate the accuracy of the model. In this work, the model of the magnetically suspended rotor is established, considering the base motions, the closed-loop control system of AMBs and gravity. The vibration response of the magnetically suspended rotor is tested on an AMB-rotor test rig mounted on a 6-DOF robot. Under three different base motion forms, the numerical simulation results based on the model are close to the experimental results, verifying the accuracy of the model. This work can provide guidance for predicting the vibration response of the magnetically suspended rotor under base motions.

Keywords: *Active magnetic bearings, Magnetically Suspended Rotor, Vibration response, Base motions*

1. Introduction

Active magnetic bearings (AMBs) have been used more and more in industrial applications due to their advantages of no friction, no lubrication, high speed, long life, and active control. The rotor supported by AMBs will inevitably be excited by the base motion brought by the moving carrier when applied in vehicle flywheels (Hawkins, et al., 2003), satellite/space-station equipment (Hawkins, et al., 2021), marine thrusters (Shen, et al., 2016), and multi-electric aero-engines (Yi, et al., 2019). There are various base motion forms, including acceleration and deceleration, vibration, sway, shock, and their combination. The results mainly display the rotor vibration. The rotor and stator will not contact when the AMB-rotor system works normally, and the rotor maintains movement between suspension clearances. However, the suspension clearance is often small, and compared with traditional mechanical bearings such as rolling or sliding bearings, the AMBs has low support stiffness and almost no overload capacity. The rotor may exceed the allowable maximum value when excited by the base motions, or even contact and rub with the touchdown bearings, cause instability and damage of the whole system. The most reliable way to investigate the stability of the magnetically suspended rotor under base motions is to conduct various vibration tests. However, it is obviously costly to conduct these tests after the design and manufacture. Therefore, it is necessary to conduct numerical simulation prediction on the vibration response of the magnetically suspended rotor after considering base motions, in order to verify its ability to resist the base excitation in the design process of the magnetically suspended rotor.

In order to evaluate the influence of earthquakes on the turbo-molecular pumps supported by the AMBs, Mural (1989) tested the vibration response of the molecular pump rotors under three seismic waves. The results showed that the AMBs can provide sufficient stiffness to ensure the molecular pump stable under earthquake conditions. Kasarda (2000) designed a single AMB mounted on a shaker to investigate the AMB bearing capacity and system natural frequency under the base sinusoidal excitation of different frequencies and amplitudes. The experimental results show that the stiffness and damping level of the AMB limits the operating performance. Zhang (2012) established a five degrees of freedom rigid rotor coupling model considering the vertical base motion, but did not further analyze its influence. Xu (2020) developed a magnetically suspended rigid rotor model considering the base translation and rotation based on the dual-frame system model, indicating that the translation motion is equivalent to the external force and the rotation motion is equivalent to the torque applied to the rotor. The effects of excitation amplitudes and pulse widths on the rotor response were analyzed by simulation, but no experimental verification was carried out. To control the lateral vibration of the flexible rotor caused by the base motion, Das (2010a, 2010b) installed an electromagnetic actuator (similar to AMB) in the middle of the rotor. The numerical simulation indicated that the rotor vibration is effectively reduced and the stability is improved. Hawkins (2018) conducted a floating shock platform test on an AMB supported chiller compressor. The compressor was subjected to a standard sequence of four different shocks generated from high explosive from different angles and distances. Three of them run normally and one of them suspended again after drop. Jarroux (2018) analyzed the influence of mass unbalance force, base motion, and nonlinear contact force of TDBs on AMB system, and carried out base harmonic excitation test. The test showed that the system could remain stable even if the rotor and TDBs were contacted by the harmonic excitation. Jarroux (2020, 2021) further evaluated the response of the magnetically suspended rotor

under strong shock excitation, and the numerical simulation predictions were consistent with the experimental results, verifying the accuracy of the model.

These studies rarely consider base rotation motions. In fact, when magnetically suspended rotating machinery is applied on ships or offshore platforms, it will be affected by waves and winds, resulting in base rolling, pitching, and yawing motions. In this paper, the finite element model of the magnetically suspended rotor under the base motions is established, in which the base motions, the closed-loop control of the AMBs and the rotor gravity load are considered. A 6-DOF robot is used to simulate the base motions of the AMB-rotor test rig, especially the base rotation motions. The dynamic response of the rotor supported by AMBs is studied by numerical simulation and experiments. The response prediction based on the finite element model is compared with the experimental results, verifying the accuracy of the model.

2. Magnetically suspended rotor model under base motions

The model of magnetically suspended rotor under base motions can be expressed as (Zhang, et al., 2023):

$$[\boldsymbol{M}]\{\ddot{\boldsymbol{q}}\} + \left([\boldsymbol{C}]_R - \dot{\phi}[\boldsymbol{G}] + [\boldsymbol{D}]_{bm}\right)\{\dot{\boldsymbol{q}}\} + ([\boldsymbol{K}] + [\boldsymbol{K}]_{bm})\{\boldsymbol{q}\} = [\boldsymbol{Q}]_{bm} + [\boldsymbol{Q}]_u + [\boldsymbol{F}]_{AMB} + [\boldsymbol{F}]_g, \tag{1}$$

where, $\{\boldsymbol{q}\}$ is the generalized coordinate of the rotor, including translation and rotation of each node. $[\boldsymbol{M}]$, $[\boldsymbol{C}]_R$, $[\boldsymbol{K}]$ are rotor mass matrix, structural damping matrix and stiffness matrix respectively. $[\boldsymbol{G}]$ is the gyroscopic effect matrix. The shrink fit components matching with AMBs and motor on the rotor are considered in modeling. $[\boldsymbol{D}]_{bm}$, $[\boldsymbol{K}]_{bm}$, $[\boldsymbol{Q}]_{bm}$ are respectively the additional damping matrix, additional stiffness matrix and additional generalized force caused by base motions. The base motions are represented by the six rigid body motions of the base. x_b, y_b, z_b, ω_x, ω_y, ω_z represent the translation along the three axes of the base coordinate system and the rotation around the three axes respectively. $[\boldsymbol{Q}]_u$ is the unbalance force. $[\boldsymbol{F}]_g$ is the gravity load. It should be noted that the base rotation will affect the distribution of gravity load in the direction of the coordinate axis. $[\boldsymbol{F}]_{AMB}$ is the electromagnetic force provided by AMBs.

The electromagnetic force is

$$f = \frac{1}{4}\mu_0 A N^2 \cos\alpha_0 \left[\left(\frac{i_0 + i_c}{C_0 - x\cos\alpha_0}\right)^2 - \left(\frac{i_0 - i_c}{C_0 + x\cos\alpha_0}\right)^2\right]. \tag{2}$$

where, μ_0 is the magnetic permeability of the vacuum, A_α is the area of a single magnetic pole, N is the number of turns in one coil, C_0 is the air gap between the rotor and the magnetic poles, x is the rotor position, i_0 is the bias current, i_c is the control current, α_0 is the angle of the magnetic pole, which represents the included angle between the direction of the electromagnetic force and the corresponding magnetic pole. For an eight poles C-type radial AMB, α_0 is usually 22.5 °. The displacement sensor and electromagnetic actuator of AMB are usually not in the same position, which needs to be considered in modeling.

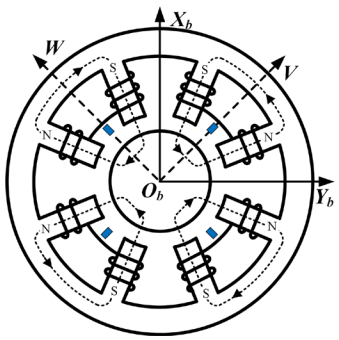

Figure 1 Schematic diagram of radial AMB.

The rotor displacement at the electromagnetic actuator can be expressed as

$$\{\boldsymbol{q}\}_b = [x_{b1} \quad y_{b1} \quad x_{b2} \quad y_{b2}]^{\mathrm{T}} = \boldsymbol{T}_B\{\boldsymbol{q}\}, \tag{3}$$

where, the transformation matrix $\boldsymbol{T}_B$ is to extract the translational displacement at the electromagnetic actuator from all generalized coordinates.

The rotor displacement at the displacement sensor can be expressed as

$$\{\boldsymbol{q}\}_{ss} = [x_{s1} \quad y_{s1} \quad x_{s2} \quad y_{s2}]^{\mathrm{T}} = \boldsymbol{T}_S\{\boldsymbol{q}\}, \tag{4}$$

where, the transformation matrix $\boldsymbol{T}_S$ is to extract the translational displacement at the displacement sensor from all generalized coordinates.

Due to the closed-loop control system of AMBs, the coil control current is obtained from the displacement detected by the displacement sensor

$$\{\boldsymbol{i}\}_c = [i_{cx1} \quad i_{cy1} \quad i_{cx2} \quad i_{cy2}]^{\mathrm{T}} = -G_s(s)G_c(s)G_a(s)\{\boldsymbol{q}\}_{ss}, \tag{5}$$

where, $G_c(s)$, $G_a(s)$, $G_s(s)$ respectively represent the transfer functions of the controller, power amplifier, and displacement sensor in the closed-loop control system. The controller adopts a conventional PID controller. The power amplifier and displacement sensor have low-pass characteristics and their transfer functions are obtained through frequency response from frequency sweep tests.

Therefore, the electromagnetic force of AMBs can be expressed as

$$[\boldsymbol{F}]_{AMB} = [f_{x1} \quad f_{y1} \quad f_{x2} \quad f_{y2}]^{\mathrm{T}}. \tag{6}$$

Based on the above model, the dynamic response of the magnetically suspended rotor under base motions is analyzed, mainly considering the situation of base rotational motion.

3. Numerical simulation and experimental results

3.1 Test rig

The AMB-rotor test rig is shown in the *Figure 2*. The rotor is 840 mm long and 5.25 kg weigh, with a first critical speed of approximately 9000 r/min. The rotor is supported by two radial AMBs (AMB1 and AMB2) and a pair of axial AMB. The main parameters of radial AMBs are shown in the *Table 1*. An induction motor is located in the middle of rotor and is used to drive the rotor to rotate. Touch down bearings (TDBs) are arranged on both sides of AMBs to temporarily support the rotor in case of failure of AMB and prevent the rotor from rubbing with stator. The gyroscopic effect of the rotor is very small. The rotor modal test, system transfer function test and unbalance response test have been carried out to verify the accuracy of the AMB-rotor model without base motions (Zhang, et al., 2023). The origin of the base coordinate system is located at the center of the AMB1.

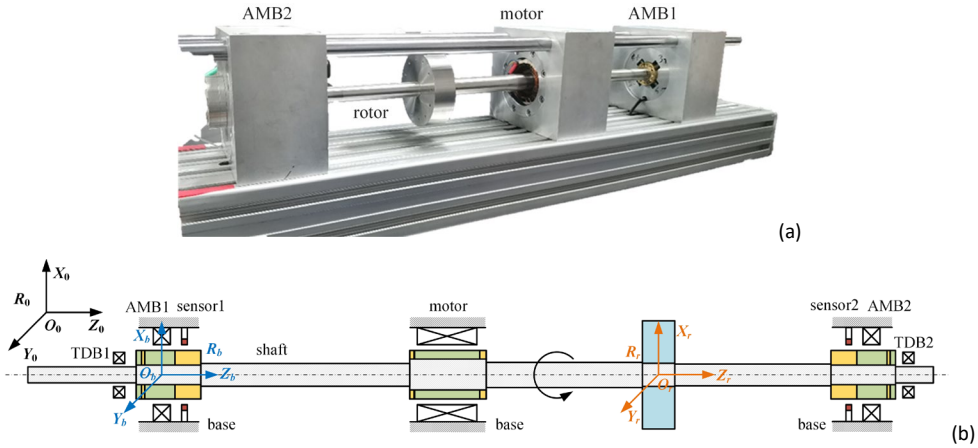

Figure 2 AMB-rotor test rig (a) Photo (b) Structure diagram.

Table 1 Parameters of radial AMBs

	Parameter	*Value*
C_0	air gap between the rotor and the magnetic poles	0.3 mm
C_{TDB}	air gap between the rotor and the TDB	0.125 mm
A_α	pole area	200 mm^2
N	number of turns	120
i_0	bias current	1.3 A

In order to simulate the base motions (such as rolling, yawing and vibration), fasten the above AMB-rotor test rig on the 6-UPS parallel robot, shown in *Figure 3*. The parallel robot can realize the movement of 6-DOF in space. The origin of the upper platform coordinate system is located at its geometric center. The base motions are simulated through the motion of the upper platform. The 6-UPS parallel robot is developed on the basis of the classic 6-DOF Stewart platform, and has the characteristics of large output torque, high motion accuracy, large stiffness, and low inertia. Both ends of each leg are connected to the upper platform and the lower platform respectively through the spherical joint and universal joint. Linear motion is driven by servo motors and screw rods. The upper and lower platforms are hexagonal with an included angle of 120 °. During the experiment, the lower platform is firmly connected to the ground and remains

stationary. The motion form of the upper platform is set, and the elongation of each support leg is obtained through dynamic inverse solution. Due to the limitation of leg elongation, while keeping the center of the upper platform stationary, the maximum angle of rotation along each axis is 20 °. Due to the limitation of the driving response speed, the minimum rotation period is 1 s.

The displacement sensors of the AMBs are used to detect the rotor displacement under the base motions. In the experiment, the rotor is only statically suspended without rotation, in order to explore the impact of base motions on the rotor vibration response. The same motions are input into the numerical model for simulation and comparison with experimental results. The test is conducted under three conditions.

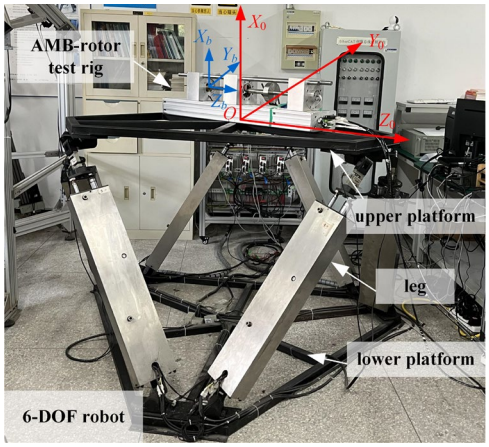

Figure 3 Experimental test rig.

3.2 Simulation and experimental results

Case 1: upper platform rotation around O_0X_0, $\alpha = \alpha_b \sin(\Omega_x t)$.

The relationship between the base and the upper platform coordinate system is shown in *Figure 4*. Then, the base motion of the AMB-rotor test rig can be derived as

$$\omega_x = \dot{\alpha} = \Omega_x \alpha_b \cos(\Omega_x t) \tag{7}$$

$$y_b = l_{0b} \sin \alpha \tag{8}$$

where, α_b and Ω_x are respectively the maximum angle and frequency of the upper platform rotation around O_0X_0, l_{0b} is the distance between the origin of the upper platform system and the origin of the stator system in the z-direction.

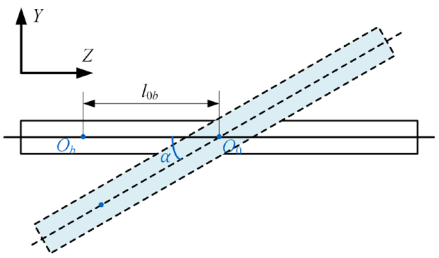

Figure 4 Schematic diagram of coordinate system relationship under the upper platform harmonic rotation around O_0X_0 (top view).

Several sets of numerical simulations and experimental verification of rotor vibration under different base rotation angles and periods were conducted. Due to the limitation of the motion range of the upper platform, the base rotation angle is set at 1-15 ° and the rotation period is 1-10 s. The results are shown in *Figure 5*. The detected rotor vibration signal has high-frequency noise because of the joint friction, signal interference and platform vibration during the operation of the 6-DOF robot. The platform has a very low rotational frequency, so the rotor vibration signal can be filtered and processed. The cut-off frequency of low-pass filter is 5 Hz, and the main frequency information can be retained, which has little impact on the results.

It can be seen that simulation and experiment can well confirm each other. As the base rotation angle and frequency increase, the vibration displacement of the rotor increases. When the rotation amplitude is 15 °, the rotor vibration noise is relatively high, which is caused by the platform. The testing standard for equipment on ships requires a yaw amplitude of 4 ° and a period of 20 s, which is much less severe than the experiments in *Figure 5*. Under this testing condition, the vibration response of the magnetically suspended rotor is very small, indicating that this test has little impact on the operation and stability of the magnetically suspended rotor.

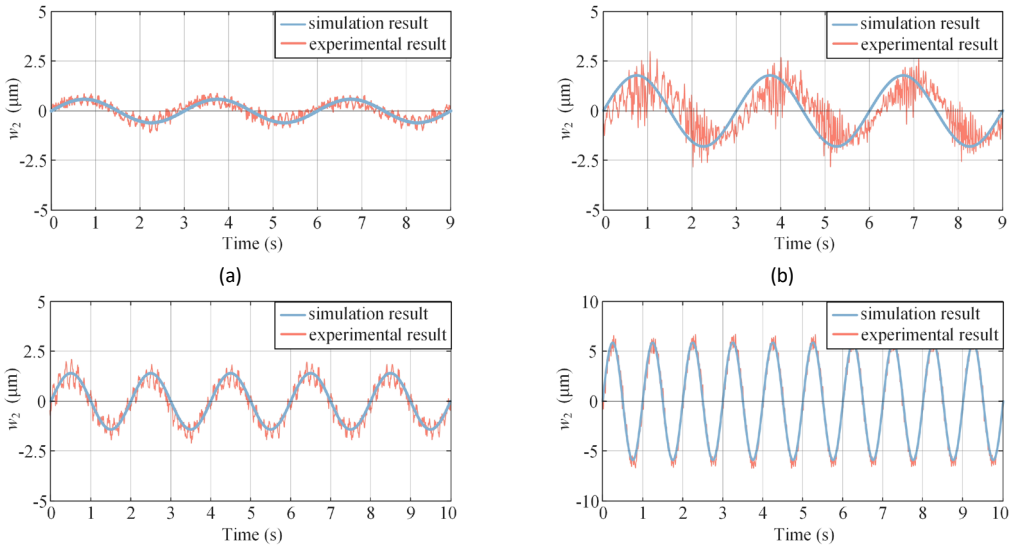

Figure 5 Simulation and experimental results of rotor vibration response under the upper platform harmonic rotation around O_0X_0 (a) 5°-3s (b) 15°-3s (c) 5°-2s (d) 5°-1s.

Case 2: upper platform rotation around O_0Z_0, $\gamma = \gamma_b \sin(\Omega_z t)$.

The relationship between the base and the upper platform coordinate system is shown in *Figure 6*. Then, the base motion of the AMB-rotor test rig can be derived as

$$\omega_z = \dot{\gamma} = \Omega_z \gamma_b \cos(\Omega_z t) \tag{9}$$

$$x_b = h_{0b} \cos\gamma \tag{10}$$

$$y_b = h_{0b} \sin\gamma \tag{11}$$

where, γ_b and Ω_z are respectively the maximum angle and frequency of the upper platform rotation around O_0Z_0, h_{0b} is the distance between the origin of the upper platform system and the origin of the stator system in the x-direction.

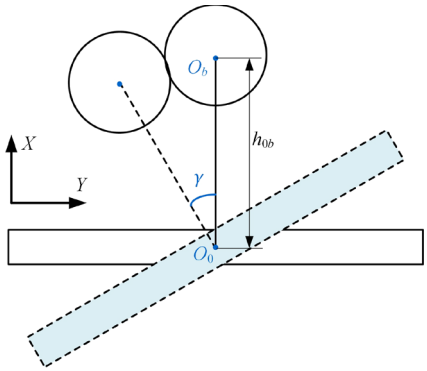

Figure 6 Schematic diagram of coordinate system relationship under the upper platform harmonic rotation around O_0Z_0 (side view).

It should be noted that in this case, the gravity load of the rotor changes. The gravity load in the x and y directions of the stator system varies periodically. When the rotor mass or rotation angle is large, the influence of gravity load distribution cannot be ignored. Taking the W-direction rotor vibration of AMB2 as the research object, several sets of numerical simulations and experimental verifications of rotor vibration under different base rotation angles and periods were conducted. According to the motion range that the platform can achieve, the rotation angle is 1-15 °, and the rotation periods is 1-10 s. The results are shown in *Figure 7*.

The rotor displacement signal in *Figure 7* was also filtered and processed. It can be seen that the simulation and experimental results are close. The experimental results are slightly larger than the simulation results, possibly due to the small rotation angle and experimental platform error, but the influence of rotation angle and frequency on rotor vibration is the same. *Figure 8* shows the rotor orbits at AMB2 when the upper platform has a rotation angle of 15 ° and a rotation period of 5 s. This base motion causes vibration in both the x and y directions of the rotor, resulting in an 8-shaped orbit. The main vibration is in the y-direction, which is about 14 μm, while the vibration in the x-direction is about 2 μm. The asymmetry of the orbit in the experiment is caused by a slight deviation between the AMB-rotor test rig and the upper platform during installation.

The standard for roll testing of equipment on ships requires an amplitude of 45 ° and a period of 5 s. The rotor orbit under this condition can be predicted through simulation, as shown in *Figure 9*. It can be seen that the maximum vibration of the rotor in the y-direction is about 40 μm and the vibration in the x-direction is about 8 μm. If h_{0b} increases, that is, the distance between the magnetically suspended rotor and the motion center of the moving carrier increases, the rotor vibration will further increase, which should be considered in the actual condition.

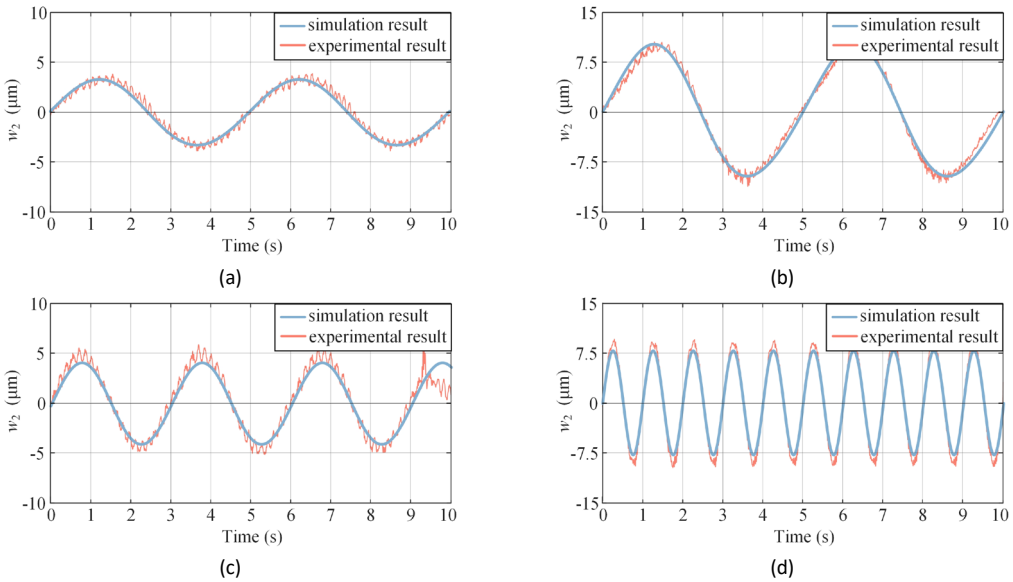

Figure 7 *Simulation and experimental results of rotor vibration response under the upper platform harmonic rotation around O_0Z_0 (a) 5°-5s (b) 15°-5s (c) 5°-3s (d) 5°-1s.*

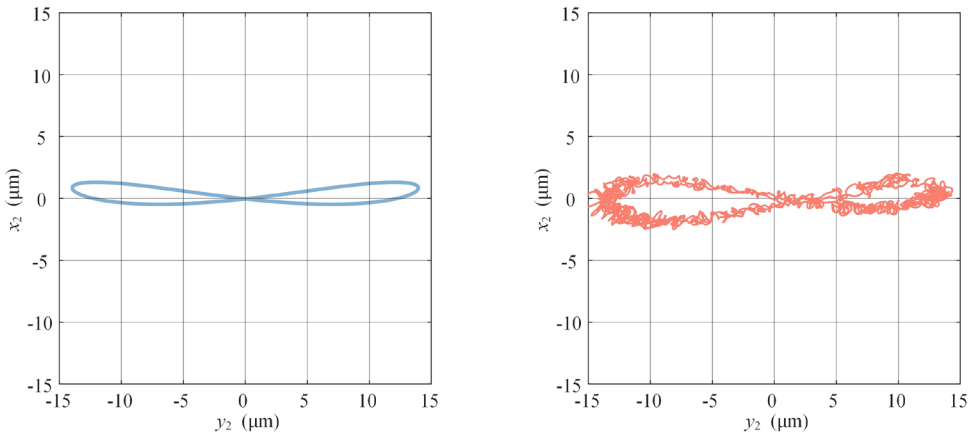

Figure 8 *Results of the rotor orbit under the upper platform harmonic rotation around O_0Z_0 with an angle of 15° and a period of 5s (a) Simulation result (b) Experimental result.*

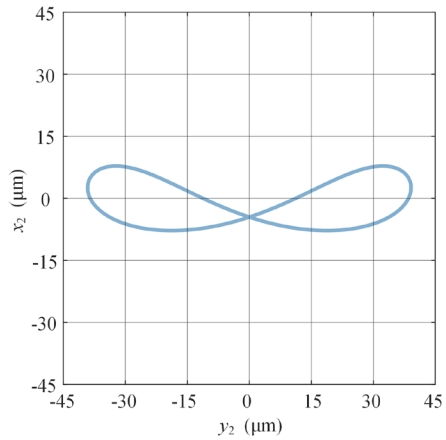

Figure 9 *Simulation results of the rotor orbit under the upper platform harmonic rotation around O_0Z_0 with an angle of 45° and a period of 5s.*

Case 3: upper platform rotation around O_0Z_0, and translation along O_0X_0 at the same time.

Results of the upper platform harmonic rotation around O_0Z_0 with an angle of 10 ° and a period of 5 s, and harmonic translation along O_0X_0 with an amplitude of 50 mm and a frequency of 1 Hz are shown in *Figure 10*. Results of the upper platform rotation around O_0Z_0 with an angle of 5 ° and a period of 3 s, and translation along O_0X_0 with an amplitude of 30 mm and a frequency of 1 Hz are shown in *Figure 11*. The simulation results accorded with the experimental results well. This composite motion makes the vibration of the rotor more complex, including signals with the same frequency as the base rotation and translation, which can be seen as the superposition of two frequency responses.

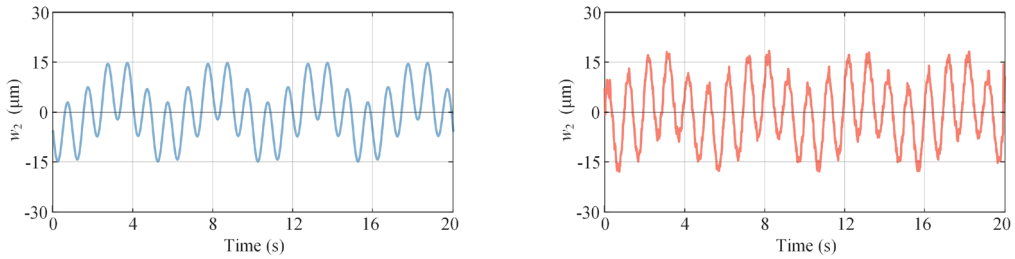

Figure 10 *Results under the upper platform rotation around O_0Z_0 with an angle of 10° and a period of 5s, and translation along O_0X_0 with an amplitude of 50mm and a frequency of 1Hz (a) Simulation result (b) Experimental result.*

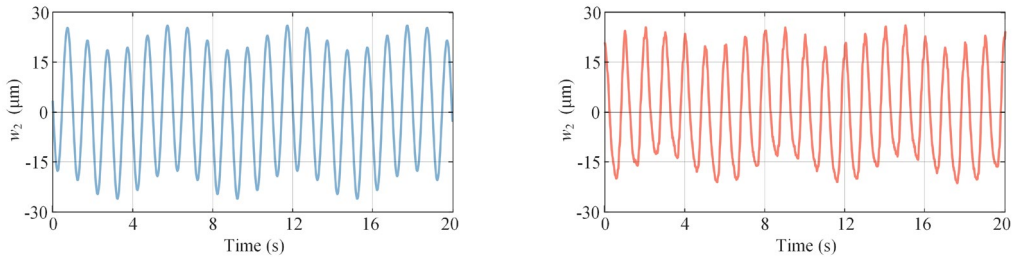

Figure 11 *Results under the upper platform rotation around O_0Z_0 with an angle of 5° and a period of 3s, and translation along O_0X_0 with an amplitude of 30mm and a frequency of 1Hz (a) Simulation result (b) Experimental result.*

4. Conclusion

The dynamic response of a magnetically suspended rotor considering base motions was investigated. Firstly, a finite element model of the magnetically suspended rotor under base motions was established, taking into account the non-collocated between the displacement sensor and the electromagnetic actuator. Then, an AMB-rotor test rig and a 6-DOF robot are used for the experiments. The 6-DOF robot can realize free motions in space to simulate the base motions of the magnetically suspended rotor, especially the base rotation. The model was verified by comparing the numerical simulation and experimental results of the rotor vibration response. That is, the rotor response under the base motion excitation can be predicted through this model. The results indicate that the rotor vibration is positively related to the maximum angle and frequency of the base rotation. When the frequency of base motion is very low, there is almost no impact on rotor vibration. The base rotation may change the rotor gravity load distribution, which cannot be ignored in the calculation of the rotor vibration response, especially when the rotor mass or the rotation angle is large.

References

Das A, Dutt J, Ray K (2010a) Active vibration control of flexible rotors on maneuvering vehicles. AIAA J. 48: 340-353.

Das A, Dutt J, Ray K (2010b) Active vibration control of unbalanced flexible rotor–shaft systems parametrically excited due to base motion. Appl. Math. Model. 34: 2353-2369.

Hawkins L, Murphy B, Zierer J, et al. (2003) Shock and vibration testing of an AMB supported energy storage flywheel. JSME Int. J. 46: 429-435.

Hawkins L, Wang Z, Nambiar K (2018) Floating shock platform testing of a magnetic bearing supported chiller compressor: Measurements and simulation results. In: Turbomachinery Technical Conference and Exposition, 11-15 June, Oslo, Norway.

Hawkins L, Filatov A, Khatri R, et al. (2021) Design of a compact magnetically levitated blower for space applications. J. Eng. Gas Turbines Power. 143.

Jarroux C, Mahfoud J, Dufour R, et al. (2018) Dynamic behavior of a rotor-AMB system due to strong base motions. In: International Conference on Rotor Dynamics. Springer, Cham.

Jarroux C, Mahfoud J, Defoy B, et al. (2020) Stability of rotating machinery supported on active magnetic bearings subjected to base excitation. J. Vib. Acoust. 142: 031004.

Jarroux C, Mahfoud J, Dufour R, et al. (2021) Investigations on the dynamic behaviour of an on-board rotor-AMB system with touchdown bearing contacts: modelling and experimentation. Mech. Syst. Signal Pr. 159: 107787.

Kasarda M, Clements J, Wicks A, et al. (2000) Effect of sinusoidal base motion on a magnetic bearing. In: IEEE International Conference on Control Applications, Anchorage, AK, USA.

Murai Y, Watanabe K, Kanemitsu Y (1989) Seismic test on turbo-molecular pumps levitated by active magnetic bearing. In: Magnetic Bearings. Springer, Berlin, Heidelberg.

Shen Y, Hu P, Jin S, et al. (2016) Design of novel shaftless pump-jet propulsor for multi-purpose long-range and high-speed autonomous

underwater vehicle. IEEE Trans. Magn. 52: 1-4.

Xu Y, Shen Q, Zhang Y, et al (2020) Dynamic modeling of the active magnetic bearing system operating in base motion condition. IEEE Access. 8: 166003-166013.

Yi Y (2019) Review and future of aircraft's propulsion type. In: Journal of Physics: Conference Series. 1345(3): 032075.

Zhang W (2012) Coupled dynamic analysis of magnetic bearing-rotor system under the influences of base motion. Appl. Mech. Mater. 109: 199-203.

Zhang Y, Zhou J, Zhang Y, et al. (2023) Modelling and vibration response of a magnetically suspended flexible rotor considering base motion. Appl. Math. Model. 118: 518-540.